

This is an Open Access document downloaded from ORCA, Cardiff University's institutional repository: <https://orca.cardiff.ac.uk/id/eprint/90066/>

This is the author's version of a work that was submitted to / accepted for publication.

Citation for final published version:

Foerster, Christian, Knight, James C., Wuest, Melinda, Rowan, Brendan, Lapi, Suzanne E., Amoroso, Angelo James, Edwards, Peter G. and Wuest, Frank 2014. Synthesis, complex stability and small animal PET imaging of a novel ^{64}Cu -labelled cryptand molecule. *MedChemComm* 5 (7), pp. 958-962. 10.1039/c4md00174e

Publishers page: <http://dx.doi.org/10.1039/c4md00174e>

Please note:

Changes made as a result of publishing processes such as copy-editing, formatting and page numbers may not be reflected in this version. For the definitive version of this publication, please refer to the published source. You are advised to consult the publisher's version if you wish to cite this paper.

This version is being made available in accordance with publisher policies. See <http://orca.cf.ac.uk/policies.html> for usage policies. Copyright and moral rights for publications made available in ORCA are retained by the copyright holders.



Synthesis, complex stability and small animal PET imaging of a novel ^{64}Cu -labelled cryptand molecule†

Christian Foerster,^a James C. Knight,^a Melinda Wuest,^a Brendan Rowan,^b Suzanne E. Lapi,^c Angelo J. Amoroso,^b Peter G. Edwards^b and Frank Wuest*^a

The radiosynthesis and radiopharmacological evaluation including small animal PET imaging of a novel ^{64}Cu -labelled cryptand molecule (^{64}Cu CryptTM) possessing a tris-pyridyl/tris-amido set of donor atoms is described.

Positron emission tomography (PET) is a rapidly expanding non-invasive molecular imaging methodology which allows high sensitivity mapping of biochemical and physiological processes at the cellular and molecular level in vivo.¹ An important aspect in the success of this technique is the use of suitably designed radiolabelled molecular probes, also referred to as PET radiotracers.²⁻⁵ Whilst the most prevalent PET radio-tracer in clinical practice is 2- ^{18}F uoro-2-deoxy-D-glucose (^{18}F FDG) for measuring glucose metabolic rate, other radiotracers like proliferation marker [^{18}F] uorothymidine (^{18}F FLT), hypoxia imaging agent [^{18}F] uoromisonidazole (^{18}F FMISO) and amino acid metabolism marker [^{11}C]methionine (^{11}C)-MET) have become clinically highly relevant PET radiotracers for various applications in oncology, neurology, and cardi-ology.^{1,5} The majority of PET radiotracers in clinical use contain short-lived positron emitters carbon-11 (^{11}C , $t_{1/2}$ ¼ 20.4 min) and uorine-18 (^{18}F , $t_{1/2}$ ¼ 109.8 min).⁴ The short half-lives of ^{11}C and ^{18}F make these radionuclides well-suited for radio-labelling small molecules as exemplified by PET radiotracers like [^{18}F]FDG, [^{18}F]FLT, [^{18}F]FMISO, and [^{11}C]MET. In contrast, higher molecular weight compounds like proteins (e.g. anti-bodies) and nanoparticles for molecular imaging and radio-therapy purposes require PET radionuclides with longer physical half-lives to accommodate the longer residence times of these larger constructs in the circulation.⁶⁻⁹

The PET radiometal copper-64 (^{64}Cu , $t_{1/2}$ ¼ 12.7 h) has been the subject of intensive research efforts for the development of both diagnostic PET radiotracers and radiotherapeutics.^{10,11} Prominent examples include hypoxia and perfusion imaging agents such as [^{64}Cu]Cu-ATSM, [^{64}Cu]Cu-PTSM, and [^{64}Cu]Cu-MTUBo respectively.

The application of ^{64}Cu as a radiometal for molecular imaging and radiotherapy requires the use of chelating agents to form kinetically inert and thermodynamically stable complexes.¹²⁻¹⁴ High complex stability is needed to obviate hydrolysis and trans-chelation to copper chelating proteins like ceruloplasmin, superoxide dismutase (SOD), metallothioneins, and copper transporting ATPases.¹⁶⁻¹⁸ Many applications utilise bifunctional chelators (BFCs) to sequester the [^{64}Cu]Cu²⁺ cation within a thermodynamically stable and kinetically inert framework while allowing attachment to selected targeting vectors (e.g. peptides, proteins). Popular and widely used BFCs for [^{64}Cu]Cu²⁺ complexation include macrocyclic chelators like 1,4,7,10-tetraazacyclododecane-1,4,7,10-tetraacetic acid (DOTA), 1,4,7-triazacyclononane-N,N⁰,N⁰⁰-triacetic acid (NOTA), and cross-ridged macrocycles like CB-TE2A.^{8,19-21} Within the class of macrocyclic chelators, cryptand molecules have been considered as particularly suitable ligands for their strong binding of Cu²⁺ cations and the kinetic inertness of the resulting complexes. Cryptands (a term derived from the greek krypt⁻e, meaning hidden) are ligands which 'entomb' metal ions like Cu²⁺ within a macrobicyclic framework. The result is often a metal complex with extraordinary thermodynamic and kinetic

^aDepartment of Oncology, University of Alberta, Edmonton, AB T6G 1Z2, Canada. E-mail: wuest@ualberta.ca; Tel: +1 780 989 8150

^bCardiff University of Wales – Department of Chemistry, Main Building, Park Place, Cardiff, CF10 3AT, UK. E-mail: amorosoaj@cardiff.ac.uk; Fax: +44 (0)29 208 74030; Tel: +44 (0)29 208 74077

^cDepartment of Radiology, Washington University School of Medicine, 510 S. Kingshighway Blvd, St. Louis, MO 63110, USA. E-mail: lapis@mir.wustl.edu; Fax: +1 314 362 9940; Tel: +1 314 362 4696

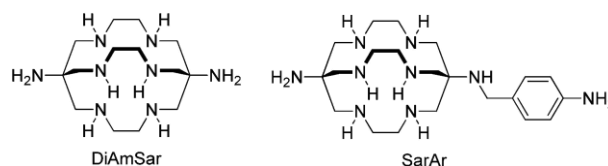


Fig. 1 Examples of Sar-type cryptands derived from sarcophagine.

stability.²² Prominent examples are cryptands derived from sarcophagine (Sar) such as DiAmSar and SarAr (Fig. 1), which form robust complexes (cryptates) with $[^{64}\text{Cu}]\text{Cu}^{2+}$ that are

highly resistant towards transchelation.

While the Sar-based cryptands offer^{22–24} excellent Cu^{2+} chelating properties, the challenging synthetic route to obtain bifunctional Sar derivatives has undoubtedly hampered their wider application within the imaging community.

Given the remarkably limited number of examples of cryptands employed for in vivo imaging applications, and considering the potential of cryptand frameworks to improve overall imaging performance with radiometal complexes, we have evaluated the cryptand molecule CryptTM as novel chelating agent for $[^{64}\text{Cu}]\text{Cu}^{2+}$ (Fig. 2). Cryptand CryptTM was prepared in good chemical yields via an elegant Pd-catalysed carbonylation reaction starting from readily available tris-aminoethylamine and tris(3-bromo-2-pyridyl)methanol. In this previous study, the crystal structure of the copper complex with CryptTM revealed the coordination of the Cu^{2+} ion to one side of the cryptand in a slightly distorted square planar coordination sphere.²⁵ CryptTM is doubly deprotonated, and the N_4 -coordination sphere of the Cu^{2+} ion involved two pyridyl and two amido N-donors. Protonation of the tertiary amine resulted in an overall 1+ charge of the $\text{Cu}(\text{II})$ -cryptate. Based on this intriguing finding, we now report the radiosynthesis and first radio-pharmacological evaluation of $[^{64}\text{Cu}]\text{Cu}$ -CryptTM complex. Radiopharmacology with $[^{64}\text{Cu}]\text{Cu}$ -CryptTM involved challenge experiments with competitive chelators EDTA (ethylenediaminetetraacetic acid) and NOTA to assess complex stability in vitro, as well as small animal PET studies in mice to assess the biodistribution profile in comparison with another, literature-reported copper-cryptate $[^{64}\text{Cu}]\text{Cu}$ -DiAmSar. The radiosynthesis and proposed structure of $[^{64}\text{Cu}]\text{Cu}$ -CryptTM is depicted in Fig. 2.

In order to optimise the ^{64}Cu complexation procedure, we explored the impact of various reaction conditions on radio-labelling yield and subsequent specific activity of $[^{64}\text{Cu}]\text{Cu}$ -CryptTM. This involved systematically altering (i) the concentration of CryptTM, (ii) type and volume of buffer solution, (iii) radioactivity concentration c_A of $[^{64}\text{Cu}]\text{Cu}(\text{OAc})_2$ in 100 mM ammonium acetate buffer (pH 5.5), and (iv) reaction temperature. The results (summarised in Table 1) clearly indicate the importance of CryptTM concentration, radioactivity concentration and reaction temperature on obtained radiochemical yield

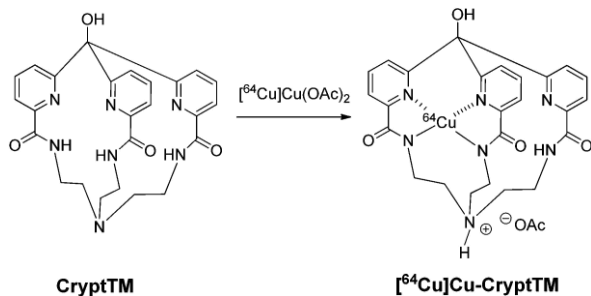


Fig. 2 Radiosynthesis of $[^{64}\text{Cu}]\text{Cu}$ -CryptTM.

and specific activity. Using low concentrations of CryptTM resulted in only moderate radiochemical yields in the range of 51–64% and low specific activities (entry 1). Increasing the CryptTM concentration up to $0.34 \text{ nmol mL}^{-1}$ gave higher radiochemical yields of 78% at 25 C.

Performance of the reaction at 37 C further increased the radiochemical yield to 95% which suggests that complexation of CryptTM with $[^{64}\text{Cu}]\text{Cu}^{2+}$ is a kinetically driven reaction (entries 2–7). Replacement of labelling buffers (1 M NH_4OAc and 1 M NaOAc) with de-ionised water also resulted in a significant increase of radiochemical yield from 78% to 98% without increasing the temperature to 37 C (entry 2 vs. 3). As a consequence, only $[^{64}\text{Cu}]\text{Cu}(\text{OAc})_2$ solution without addition of buffer solution or de-ionised water was used in further experiments (entries 4–7).

In all cases, radiochemical yields exceeded 95% at 37 C. High specific activities of up to 16 GBq mmol^{-1} were achieved by lowering cryptand concentration to $0.25 \text{ nmol mL}^{-1}$ while increasing radioactivity concentration to 4000 kBq mL^{-1} (entry 7). High specific activities were obtained without the implementation of purification steps. Radiolabelling of very low quantities of CryptTM (1.0 nmol to 4.5 nmol) with up to 100 MBq of $[^{64}\text{Cu}]\text{Cu}(\text{OAc})_2$ gave higher specific activities of $\#45 \text{ GBq mmol}^{-1}$ (corrected to recovered radioactivity after solid-phase extraction purification as radiochemical yields decreased below 95%). The optimised reaction conditions for complexation of $[^{64}\text{Cu}]\text{Cu}^{2+}$ by CryptTM are compatible with structural and functional integrity of delicate biopolymers like CryptTM-functionalised peptides and proteins as prospective targeting vectors for molecular imaging purposes.

Based on previous density functional theory (DFT) calculations, CryptTM has also been proposed to form complexes with trivalent cations like $\text{In}(\text{III})$, $\text{Y}(\text{III})$, and $\text{Ga}(\text{III})$.²⁵ However, our radiolabelling experiments with $[^{68}\text{Ga}]\text{Ga}^{3+}$ obtained from a $^{68}\text{Ge}/^{68}\text{Ga}$ generator did not result in the formation of a stable $[^{68}\text{Ga}]\text{Ga}$ -CryptTM complex despite applying a variety of labelling conditions as assessed by radio-TLC and radio-HPLC analysis (data not shown).

The next set of experiments dealt with the investigation of $[^{64}\text{Cu}]\text{Cu}$ -CryptTM stability in vitro in direct comparison with literature-reported $[^{64}\text{Cu}]\text{Cu}$ -DiAmSar by means of challenge experiments involving chelators EDTA ($\log K_{\text{Cu-EDTA}} \approx 18.5$) and NOTA ($\log K_{\text{Cu-NOTA}} \approx 21.6$).²⁶ $[^{64}\text{Cu}]\text{Cu}$ -CryptTM and $[^{64}\text{Cu}]\text{Cu}$ -DiAmSar were challenged with competitive chelators EDTA and NOTA at stoichiometric ratios of 1 : 1 and 1 : 100 and were subsequently tested for transchelation of $[^{64}\text{Cu}]\text{Cu}^{2+}$ by radio-TLC. Challenge experiments were performed at 25 C. The results are summarised in Table 2.

In the case of $[^{64}\text{Cu}]\text{Cu}$ -CryptTM substantial transchelation was observed in the presence of chelators EDTA and NOTA when compared to $[^{64}\text{Cu}]\text{Cu}$ -DiAmSar. $[^{64}\text{Cu}]\text{Cu}$ -DiAmSar was inert towards transchelation with EDTA and NOTA over the entire course of the experiment (up 18 h). This is consistent with the reported high kinetic inertness of $[^{64}\text{Cu}]\text{Cu}$ -Sar complexes.^{22–24}

Challenge experiments of $[^{64}\text{Cu}]\text{Cu}$ -CryptTM with EDTA and NOTA gave higher rates of transchelation with EDTA for both

Table 1 Systematic optimisation of ^{64}Cu -labelling conditions for CryptTM (time of radiolabelling was 60 min for each experiment)^a

Entry	Buffer	Concentration of CryptTM [nmol mL ⁻¹]	Activity concentration cA [kBq mL ⁻¹]	Temperature [°C]	Radiochemical yield [%]	Specific activity As [GBq mmol ⁻¹]
1	100 mL (A)	0.22	352	25	64.3	0.10
	100 mL (B)				68.4	0.11
	100 mL (C)				51.2	0.08
2	20 mL (B)	0.34	470.0	25	78.6	0.11
					37	95.3
3	20 mL (D)	0.34	72	25	98	0.20
4	no buffer added	0.46	200.10	37	>99*	0.44
5	no buffer added	0.46	1300.50	37	>99*	2.84
6	no buffer added	0.58	3684.526	37	>95	6.36–0.91
7	no buffer added	0.25	4091.455	37	>95	16.36–1.82

^a A 1 M ammonium acetate pH 5.0, B 1 M ammonium acetate pH 6.0, C 1 M sodium acetate pH 6.0, D de-ionized water, * 10 uL deionized water/ buffer/PBS was added at the end of the reaction as result of solvent evaporation during radiolabeling procedure at 37 °C.

Table 2 Challenge experiments of [^{64}Cu]Cu–CryptTM and [^{64}Cu]Cu–DiAmSar with EDTA and NOTA (ratios refer to CryptTM/DiAmSar-to-EDTA or NOTA). Listed percentages refer to intact [^{64}Cu]Cu–CryptTM or [^{64}Cu]Cu–DiAmSar, respectively, as determined by radio-TLC ($R_{f, \text{DiAmSar-EDTA}} \frac{1}{4} 0.8$; $R_{f, \text{DiAmSar-NOTA}} \frac{1}{4} 0.5$; $R_{f, \text{DiAmSar-CryptTM}} \frac{1}{4} 0.0$; $R_{f, \text{CryptTM}} \frac{1}{4} 0.0$)

Time	EDTA challenge of [^{64}Cu]Cu–CryptTM		NOTA challenge of [^{64}Cu]Cu–CryptTM		EDTA challenge of [^{64}Cu]Cu–DiAmSar		NOTA challenge of [^{64}Cu]Cu–DiAmSar	
	1 : 1	1 : 100	1 : 1	1 : 100	1 : 1	1 : 100	1 : 1	1 : 100
10 min	46%	34%	74%	25%	100%	100%	100%	100%
40 min	24%	18%	53%	12%	100%	100%	100%	100%
18 h	11%	7%	9%	0%	100%	100%	100%	100%

used stoichiometric ratios (1 : 1 and 1 : 100) within the first 40 min of the experiment. This finding is surprising as Cu(II)–EDTA complex exhibits a thermodynamic complex stability constant three magnitudes lower compared to that of the Cu(II)–NOTA complex. Presumably, acyclic EDTA seems to be more flexible in changing its three-dimensional conformation leading to kinetically more preferred transfer of [^{64}Cu]Cu²⁺ from [^{64}Cu]Cu–CryptTM to EDTA rather than from [^{64}Cu]Cu–CryptTM to NOTA. However, after 18 h, no intact [^{64}Cu]Cu–CryptTM was detectable when a 1 : 100 excess of NOTA was used for the challenge experiment. Under the same conditions, 7% of intact [^{64}Cu]Cu–CryptTM was found after 18 h for the challenge experiment with EDTA. Notably, the rate of trans-chelation seems to be less affected by the concentration of EDTA when compared with NOTA. Trans-chelation of [^{64}Cu]Cu–CryptTM with EDTA tends to occur rapidly within the first 40 min, and significant trans-chelation was observed during this period of time. The amount of remaining intact complex after 40 min was comparable (24% and 18%) for both tested stoichiometric ratios (1 : 1 and 1 : 100, respectively). Rate of trans-chelation of [^{64}Cu]Cu–CryptTM in the presence of NOTA was more dependent on the ratio of the two chelators. At a 1 : 1 ratio of [^{64}Cu]Cu–CryptTM to NOTA, 74% (10 min), 53% (40 min), and 9% (18 h) of intact [^{64}Cu]Cu–CryptTM was detected. Significantly lower amounts of intact

[^{64}Cu]Cu–CryptTM were found at a 1 : 100 ratio between [^{64}Cu]Cu–CryptTM and NOTA.

These results suggest kinetically-driven trans-chelation of [^{64}Cu]Cu–CryptTM with structurally flexible acyclic EDTA chelator, whereas the driving force for trans-chelation of [^{64}Cu]Cu–CryptTM with macrocyclic NOTA chelator seems to be the formation of thermodynamically more stable [^{64}Cu]Cu–NOTA complex.

Radiopharmacological evaluation of [^{64}Cu]Cu–CryptTM in murine blood samples provided data on distribution pattern of radioactivity in blood cells, plasma proteins, and plasma at different time points (Fig. 3). Results in Fig. 3 revealed low binding of radioactivity (15%) on blood cells at all investigated time points (5, 30, and 60 min). Increasing amounts of radio-activity were found in plasma protein fraction of murine blood which exceeded 70% of radioactivity in whole blood pool at 60 min. Consequently, radioactivity in plasma dropped over time, reaching 18% after 60 min post injection (p.i.). Radio-TLC analysis of plasma fractions indicated intact [^{64}Cu]Cu–CryptTM as administered intravenously at all points. The high plasma protein binding may be indicative of trans-chelation of [^{64}Cu]Cu²⁺ to plasma proteins, and/or binding of intact [^{64}Cu]Cu–CryptTM to plasma proteins.

Radiopharmacological profile of [^{64}Cu]Cu–CryptTM was further elucidated with dynamic small animal PET imaging in

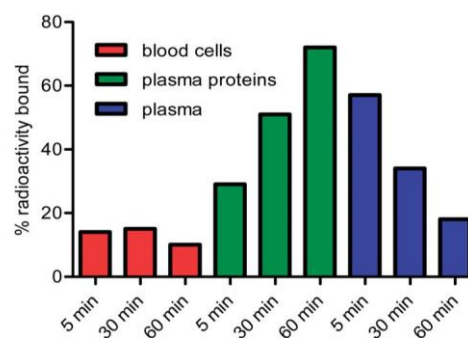


Fig. 3 Distribution of radioactivity in murine blood compartments after intravenous injection of [^{64}Cu]Cu–CryptTM into normal mouse.

comparison to $[^{64}\text{Cu}]\text{Cu-DiAmSar}$. In Fig. 4, representative PET images of $[^{64}\text{Cu}]\text{Cu-CryptTM}$ (Fig. 4A) and $[^{64}\text{Cu}]\text{Cu-DiAmSar}$ (Fig. 4B) at 5, 15, and 60 min p.i. into EMT6 tumor-bearing BALB/c mice.

After injection of $[^{64}\text{Cu}]\text{Cu-CryptTM}$ and its initial distribution phase, the majority of radioactivity was rapidly eliminated from the blood pool and cleared through the hepatobiliary elimination pathway. Radioactivity was also observed in the bladder during the perfusion phase. Over time, $[^{64}\text{Cu}]\text{Cu-CryptTM}$ demonstrated predominantly hepatobiliary excretion accompanied by an almost constant accumulation and retention of radioactivity in liver tissue over time (Fig. 5). The determined distribution and clearance pattern in the case of $[^{64}\text{Cu}]\text{Cu-CryptTM}$ is consistent with the known tendency of pyridine derivatives to be subject of metabolism in liver cells by N-methyltransferases as well as monooxygenase cytochrome P450.²⁷⁻³⁰

Moreover, the predominantly hepatobiliary excretion pathway of $[^{64}\text{Cu}]\text{Cu-CryptTM}$ also leads to exposure to liver enzyme superoxide dismutase as a potential site for trans-chelation of $^{64}\text{Cu}^{2+}$ resulting in accumulation and retention of radioactivity in the liver over time. This observation is also consistent with the results of the challenge experiments in this work (see Table 2) suggesting a substantial kinetic instability of $[^{64}\text{Cu}]\text{Cu-CryptTM}$ towards trans-chelation. In contrast to $[^{64}\text{Cu}]\text{Cu-CryptTM}$, $[^{64}\text{Cu}]\text{Cu-DiAmSar}$ was cleared almost exclusively through the kidneys, and the majority of radioactivity was found in the bladder after 60 min p.i. The low uptake and rapid clearance of $[^{64}\text{Cu}]\text{Cu-DiAmSar}$ from the liver confirms high kinetic inertness of the complex towards trans-chelation in vivo. However, the very fast elimination from blood system possibly denies de nite assessment of in vivo stability due to very short time of interaction with competitive endogenous ligands. The observed differences in the biodistribution and elimination pattern of $[^{64}\text{Cu}]\text{Cu-CryptTM}$ and $[^{64}\text{Cu}]\text{Cu-DiAmSar}$ are in principle agreement with the determined

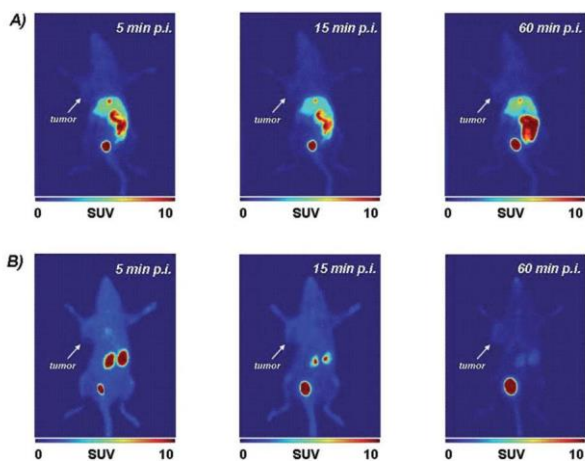


Fig. 4 PET images (maximum intensity projection) of $[^{64}\text{Cu}]\text{Cu-CryptTM}$ (A) and for $[^{64}\text{Cu}]\text{Cu-DiAmSar}$ (B) at selected time points after single intravenous injection (5 MBq for each complex) into EMT-6 tumor-bearing BALB/c mice.

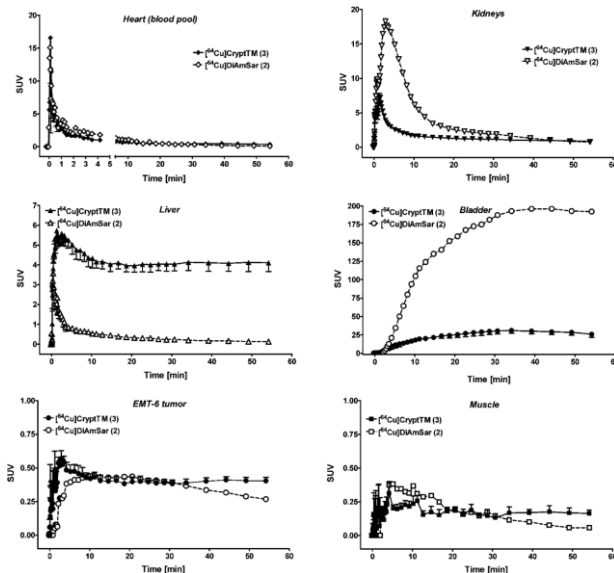


Fig. 5 Time-activity-curves of blood, kidneys, liver, bladder, tumour, and muscle after injection of $[^{64}\text{Cu}]\text{Cu-CryptTM}$ and $[^{64}\text{Cu}]\text{Cu-DiAmSar}$ into EMT6-tumour bearing BALB/c mice.

differences in kinetic stability and lipophilicity of both complexes. Lipophilicity was determined according to the shake-ask method resulting in log P values of 0.3 and 3.7 at physiological pH of 7.4 for $[^{64}\text{Cu}]\text{Cu-CryptTM}$ and $[^{64}\text{Cu}]\text{Cu-DiAmSar}$, respectively.

Fig. 5 summarises all time-activity-curves for radioactivity uptake profiles from the heart (blood pool), liver, kidneys, bladder, tumour and muscle visualising different bio-distribution and clearance patterns after injection of both ^{64}Cu -labelled complexes. For $[^{64}\text{Cu}]\text{Cu-CryptTM}$ experiments we also calculated standardised uptake values (SUV) in EMT6-tumour tissue and muscle at which $\text{SUV}_{\text{tumour}} \approx 0.40 \pm 0.03$ ($n \approx 3$) was significantly higher compared to $\text{SUV}_{\text{muscle}} \approx 0.16 \pm 0.02$ ($n \approx 3$) after 60 min p.i. Injection of $[^{64}\text{Cu}]\text{Cu-CryptTM}$ led to a retention of radioactivity in EMT6-tumour tissue; however, overall uptake levels were comparable with previous experiments using $[^{64}\text{Cu}]\text{Cu(OAc)}_2$. This finding is indicative of non-specific accumulation of radioactivity in EMT6 tumours.

Conclusions

We have prepared and evaluated a novel ^{64}Cu -labelled cryptand molecule ($[^{64}\text{Cu}]\text{Cu-CryptTM}$). Radiopharmacological profile of $[^{64}\text{Cu}]\text{Cu-CryptTM}$ was studied in comparison with $[^{64}\text{Cu}]\text{Cu-DiAmSar}$ as 'gold standard' for kinetically inert ^{64}Cu -labelled cryptand molecules. Radiopharmacological evaluation of $[^{64}\text{Cu}]\text{Cu-CryptTM}$ revealed insufficient kinetic stability which is consistent with the assumed unfavourable coordination mode of $[^{64}\text{Cu}]\text{Cu}^{2+}$ through two pyridyl and two amido donors as determined by crystal structure. However, the facile synthetic access to the novel cryptand CryptTM and related structures, and its favourable complex formation conditions using $[^{64}\text{Cu}]\text{Cu(OAc)}_2$ warrant further investigation of related CryptTM-type

molecules possessing a more favourable tri-pyridyl/tri-amine donor group set to allow formation of more kinetically inert ^{64}Cu -cryptates.

References

- 1 S. S. Gambhir, *Nat. Rev. Cancer*, 2002, 2, 683–693.
- 2 S. L. Pimlott and A. Sutherland, *Chem. Soc. Rev.*, 2011, 40, 149–162.
- 3 S. M. Ametamey, M. Honer and P. A. Schubiger, *Chem. Rev.*, 2008, 108, 1501–1516.
- 4 P. W. Miller, N. J. Long, R. Vilar and A. D. Gee, *Angew. Chem., Int. Ed.*, 2008, 47, 8998–9033.
- 5 S. S. Gambhir, J. Czernin, J. Schwimmer, D. H. S. Silverman, R. E. Coleman and M. E. Phelps, *J. Nucl. Med.*, 2001, 42, 1S–93S.
- 6 B. M. Zeglis, J. L. Houghton, M. J. Evans, N. Viola-Villegas and J. S. Lewis, *Inorg. Chem.*, 2014, 53, 1880–1899.
- 7 T. J. Wadas, E. H. Wong, G. R. Weisman and C. J. Anderson, *Chem. Rev.*, 2010, 110, 2858–2902.
- 8 E. W. Price and C. Orvig, *Chem. Soc. Rev.*, 2014, 43, 260–290.
- 9 Y. Zhou, K. E. Baidoo and M. W. Brechbiel, *Adv. Drug Delivery Rev.*, 2013, 65, 1098–1111.
- 10 M. R. Lewis, M. Wang, D. B. Axworthy, L. J. Theodore, R. W. Mallet, A. R. Fritzberg, M. J. Welch and C. J. Anderson, *J. Nucl. Med.*, 2003, 44, 1284–1292.
- 11 J. M. Connett, C. J. Anderson, L. W. Guo, S. W. Schwarz, K. R. Zinn, B. E. Rogers, B. A. Siegel, G. W. Philpott and M. J. Welch, *Proc. Natl. Acad. Sci. U. S. A.*, 1996, 93, 6814–6818.
- 12 A. L. Vavere and J. S. Lewis, *Dalton Trans.*, 2007, 4893–4902.
- 13 J. C. Knight, M. Wuest, F. A. Saad, M. Wang, D. W. Chapman, H.-S. Jans, S. E. Lapi, B. M. Kariuki, A. J. Amoroso and F. Wuest, *Dalton Trans.*, 2013, 42, 12005–12014.
- 14 C. J. Mathias, M. J. Welch, D. J. Perry, A. H. McGuire, X. Zhu, J. M. Connett and M. A. Green, *Int. J. Radiat. Appl. Instrum., Part B*, 1991, 18, 807–811.
- 15 C. J. Anderson and R. Ferdani, *Cancer Biother. Radiopharm.*, 2009, 24, 379–393.
- 16 R. M. Reilly, *Monoclonal Antibody and Peptide-Targeted Radiotherapy of Cancer*, WILEY-BLACKWELL, Hoboken, New Jersey, 1st edn, 2010.
- 17 C. J. Anderson, L. A. Jones, L. A. Bass, E. L. C. Sherman, D. W. McCarthy, P. D. Cutler, M. V. Lanahan, M. E. Cristel, J. S. Lewis and S. W. Schwarz, *J. Nucl. Med.*, 1998, 39, 1944–1951.
- 18 T. J. Wadas, E. H. Wong, G. R. Weisman and C. J. Anderson, *Curr. Pharm. Des.*, 2007, 13, 3–16.
- 19 C. A. Boswell, X. Sun, W. Niu, G. R. Weisman, E. H. Wong, A. L. Rheingold and C. J. Anderson, *J. Med. Chem.*, 2004, 47, 1465–1474.
- 20 S. Ait-Mohand, P. Fournier, V. Dumulon-Perreault, G. E. Kiefer, P. Jurek, C. L. Ferreira, F. B´enard and B. Gu´erin, *Bioconjugate Chem.*, 2011, 22, 1729–1735.
- 21 C. L. Ferreira, D. T. T. Yapp, S. Crisp, B. W. Sutherland, S. S. W. Ng, M. Gleave, C. Bensimon, P. Jurek and G. E. Kiefer, *Eur. J. Nucl. Med. Mol. Imaging*, 2010, 37, 2117–2126.
- 22 N. M. Di Bartolo, A. M. Sargeson, T. M. Donlevy and S. V. Smith, *J. Chem. Soc., Dalton Trans.*, 2001, 2303–2309.
- 23 S. Liu, D. Li, C.-W. Huang, L.-P. Yap, R. Park, H. Shan, Z. Li and P. S. Conti, *Theranostics*, 2012, 2, 589–596.
- 24 E. Mume, A. Asad, N. M. Di Bartolo, L. Kong, C. Smith, A. M. Sargeson, R. Price and S. V. Smith, *Dalton Trans.*, 2013, 42, 14402–14410.
- 25 J. C. Knight, R. Prabakaran, B. D. Ward, A. J. Amoroso, P. G. Edwards and B. M. Kariuki, *Dalton Trans.*, 2010, 39, 10031–10033.
- 26 A. Bevilacqua, R. I. Gelb, W. B. Hebard and L. J. Zompa, *Inorg. Chem.*, 1987, 26, 2699–2706.
- 27 R. Gu, D. E. Hibbs, J. A. Ong, R. J. Edwards and M. Murray, *Biochem. Pharmacol.*, 2014, 88, 245–252.
- 28 H. Lu, X. Huang, M. D. M. Abdulhameed and C.-G. Zhan, *Bioorg. Med. Chem.*, 2014, 22, 2149–2156.
- 29 S. C. Khojasteh, Q. Yue, S. Ma, G. Castanedo, J. Z. Chen, J. Lyssikatos, T. Mulder, R. Takahashi, J. Ly, K. Messick, W. Jia, L. Liu, C. E. C. A. Hop and H. Wong, *Drug Metab. Dispos.*, 2014, 42, 343–351.
- 30 Z. H. Milani, D. B. Ramsden and R. B. Parsons, *J. Biochem. Mol. Toxicol.*, 2013, 27, 451–456.